JACS
JOURNAL OF THE AMERICAN CHEMICAL SOCIETY
Article
pubs.acs.org/JACS

Constructing Solid–Gas-Interfacial Fenton Reaction over Alkalinized-C_3N_4 Photocatalyst To Achieve Apparent Quantum Yield of 49% at 420 nm

Yunxiang Li,[†,‡] Shuxin Ouyang,*[,†,‡,§] Hua Xu,[†,‡,§] Xin Wang,[†,‡] Yingpu Bi,[#] Yuanfang Zhang,[†,‡] and Jinhua Ye*[,†,‡,§,∥]

[†]TU-NIMS Joint Research Center, School of Materials Science and Engineering, Tianjin University, Tianjin 300072, PR China
[‡]Collaborative Innovation Center of Chemical Science and Engineering (Tianjin), Tianjin 300072, PR China
[§]Key Lab of Advanced Ceramics and Machining Technology, Ministry of Education, Tianjin 300072, PR China
[#]State Key Laboratory for Oxo Synthesis & Selective Oxidation and National Engineering Research Center for Fine Petrochemical Intermediates, Lanzhou Institute of Chemical Physics, CAS, Lanzhou 730000, PR China
[∥]International Center for Materials Nanoarchitectonics (WPI-MANA) and Environmental Remediation Materials Unit, National Institute for Materials Science (NIMS), Tsukuba 305-0047, Japan

Supporting Information

ABSTRACT: Efficient generation of active oxygen-related radicals plays an essential role in boosting advanced oxidation process. To promote photocatalytic oxidation for gaseous pollutant over g-C_3N_4, a solid–gas interfacial Fenton reaction is coupled into alkalinized g-C_3N_4-based photocatalyst to effectively convert photocatalytic generation of H_2O_2 into oxygen-related radicals. This system includes light energy as power, alkalinized g-C_3N_4-based photocatalyst as an in situ and robust H_2O_2 generator, and surface-decorated Fe^{3+} as a trigger of H_2O_2 conversion, which attains highly efficient and universal activity for photodegradation of volatile organic compounds (VOCs). Taking the photooxidation of isopropanol as model reaction, this system achieves a photoactivity of 2–3 orders of magnitude higher than that of pristine g-C_3N_4, which corresponds to a high apparent quantum yield of 49% at around 420 nm. In-situ electron spin resonance (ESR) spectroscopy and sacrificial-reagent incorporated photocatalytic characterizations indicate that the notable photoactivity promotion could be ascribed to the collaboration between photocarriers (electrons and holes) and Fenton process to produce abundant and reactive oxygen-related radicals. The strategy of coupling solid–gas interfacial Fenton process into semiconductor-based photocatalysis provides a facile and promising solution to the remediation of air pollution via solar energy.

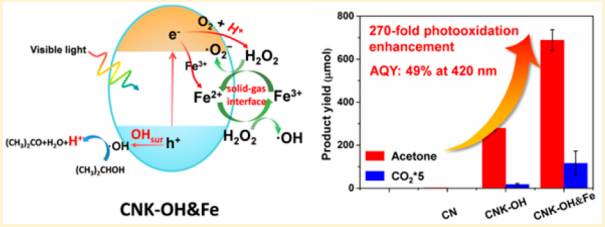

INTRODUCTION

Constructing efficient photocatalytic system is one of the noble missions in the fields of photochemistry and materials science, because photocatalysis provides a promising and alternative solution for realizing environmental remediation and counteracting energy shortage via solar energy.[1−4] Since graphite-phase C_3N_4 (g-C_3N_4) was developed as a metal-free visible-light-sensitive photocatalyst in 2009,[5] it has drawn considerable and increasing attention due to its rapidly extended applications in all kinds of photocatalytic branches, such as H_2/O_2 evolution from water splitting,[6−9] contaminant elimination,[10,11] CO_2 reduction,[12,13] and so on.[14,15] The unique chemical composition and crystal structure endow g-C_3N_4 with great adjustability and compatibility, and thus, a series of efficient photocatalytic systems for H_2 evolution[8,16,17] and organic dye degradation[10,11] have been constructed via g-C_3N_4-based materials. However, as for solid–gas-interfacial heterocatalysis over g-C_3N_4-based materials, the photocatalytic efficiency is still relatively low, especially for volatile organic compounds (VOCs) removal (Supporting Information, Table S1).[18−21]

The fundamental of organic pollutant photodegradation is a free radical chain reaction.[22,23] Direct and effective approach to enhance photoactivity for VOCs degradation over g-C_3N_4 is to generate abundant and active oxygen-related species on its surface. It is well-known that Fenton reaction can produce particularly plenty oxygen-related species via the reaction between Fe^{3+}/Fe^{2+} pair and H_2O_2 as below:[24,25]

$$Fe^{2+} + H_2O_2 \rightarrow Fe^{3+} + \cdot OH + OH^- \quad (1)$$

$$Fe^{3+} + H_2O_2 \rightarrow Fe^{2+} + \cdot OOH + H^+ \quad (2)$$

In almost all cases, however, either classic Fenton reaction or other modes of Fenton process is dependent on a suitable acid aqueous-phase medium (pH = 2.5–5.0) to realize efficient

Received: July 14, 2016
Published: September 19, 2016

DOI: 10.1021/jacs.6b07272
J. Am. Chem. Soc. 2016, 138, 13289–13297

reactivity,[26−28] since Fe^{3+} is easy to be converted into complex forms under strong acid or alkaline conditions and thus to reduce reaction performance:[25]

$$\text{strong acid condition: } Fe^{3+} + 6H_2O \leftrightarrow Fe(H_2O)_6^{3+} \quad (3)$$

$$\text{alkaline condition: } Fe^{3+} \leftrightarrow FeOH^{2+} \leftrightarrow Fe(OH)_2^{+} \leftrightarrow Fe_2(OH)_2^{4+} \leftrightarrow \text{other polynuclear species} \leftrightarrow Fe_2O_3 \cdot nH_2O(s) \quad (4)$$

How can Fenton process be operated at solid−gas interface? Some photocatalysts are capable of producing H_2O_2 under light irradiation, which supplies the prerequisite to initiate Fenton process; however, previous study[29,30] and our attempt (Supporting Information, Figure S1) indicate that simple Fe^{3+} modification over photocatalyst (including g-C_3N_4) exhibits limited enhancement or even reduction effect on photoactivity. Therefore, it is inferred that a suitable chemical environment of g-C_3N_4 surface to adapt efficient Fenton reaction is the key issue to achieve its effective VOCs degradation.

In this article, we report an alkalinized g-C_3N_4-based photocatalyst with Fe^{3+} loading to construct solid−gas interfacial Fenton reaction which can produce considerably abundant oxygen-related radicals to participate photocatalytic reaction. Unexpectedly, differing from traditional aqueous-medium Fenton reaction, an alkaline but not acid surface offers appropriate chemical environment for such solid−gas interfacial Fenton process. This photocatalytic system exhibits highly efficient and universal activity for photodegradation of volatile organic compounds (VOCs). In particular, compared to pristine g-C_3N_4, the photodegradation rate of isopropanol via this photocatalytic system has achieved a 270-fold magnification, which corresponds to a high apparent quantum yield of 49% at around 420 nm. The significant photoactivity enhancement could be attributed to a three-step cascading reaction to produce reactive radicals as following: (1) the surface hydroxyl groups are activated by photoholes to generate hydroxyl radicals which oxidize VOCs to produce protons; (2) the O_2 and protons evolve into H_2O_2 via a two-photoelectron reduction process; (3) the Fe^{2+}/Fe^{3+} pair reacts with the H_2O_2 to provide oxygen-related radicals. The proposed material surface modulation coupled with solid−gas interfacial Fenton reaction may open a new route for the efficient production of active radicals at photocatalyst surface, which therefore significant promotes photocatalytic oxidation.

RESULTS AND DISCUSSION

Formation of Hydroxyl and Fe^{3+} Species Modified g-C_3N_4. The pristine g-C_3N_4 (denoted as CN) was fabricated using a common method of melamine thermal polymerization.[31] To enhance the carrier transfer efficiency and graft the hydroxyl groups, some amounts of KCl and NaOH were added into the feedstock (named as CNK and CNK−OH, respectively) following the method of our previous study.[32] Further ferric modification was realized by an impregnation method over the CNK−OH sample. As presented in Figure 1, the X-ray diffraction (XRD) pattern of the CN displays two typical diffraction peaks at around 27.4° and 13.0°. For the samples modified with KCl, their phases kept the same with CN. However, it slightly shifts relative to CN from 27.4° to 27.9° and 28.1° for CNK and CNK−OH, respectively. It means that the interlayer distance of the (002) plane decreased after

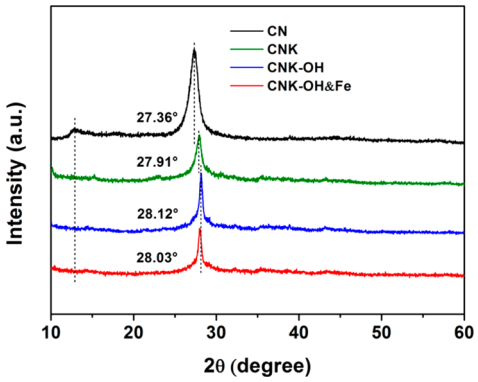

Figure 1. XRD patterns of as-prepared samples.

modification with KCl. Together with the absence of (100) signal at 13.0°, it suggests that K^+ may be embedded into the in-planes of CN sheet and cause attractive interaction between K and N, which can be further corroborated by the K 2*p* spectrum of XPS characterization (Figure 1 and Figure S2). In the K incorporated samples, the peak at 292.86 eV presents the specific feature of N−K bonds just like that in KN_3 (292.74 eV);[33] such N−K bonding in g-C_3N_4 should be the form of K linking to N atoms in different layers. As illustrated above, the interlayer ions will alter the distance of layers due to the interaction between ions and layer. However, the Fe^{3+} loading barely affects the XRD diffraction peaks, indicating that Fe^{3+} ions modify sample limited to the region of shallow surface.

To determine the hydroxyl groups over the samples, the measurements of Fourier transform-infrared (FT-IR) and electron spin resonance (ESR) spectroscopies were applied (Figure 2). Three extra bands at 1000, 1158, 2152 cm^{-1} appear

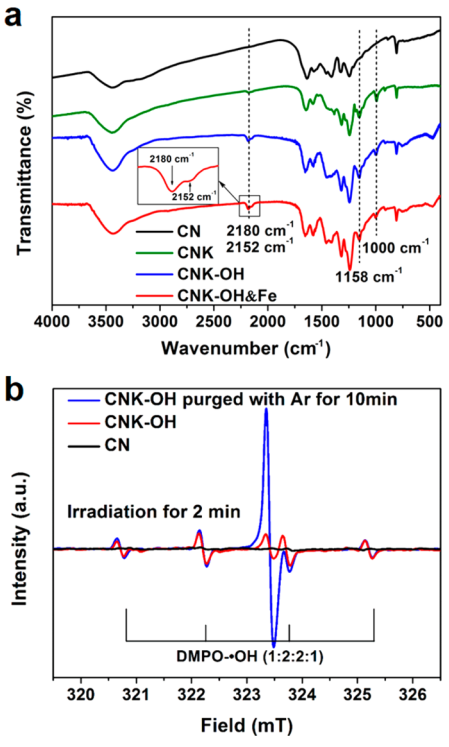

Figure 2. (a) FT-IR spectra of the as-prepared samples. (b) ESR spectra of DMPO-spin adduct measured in the aqueous solution of samples exposed to visible light (420 nm < λ < 800 nm).

DOI: 10.1021/jacs.6b07272
J. Am. Chem. Soc. 2016, 138, 13289−13297

when KCl was introduced in synthesis (Figure 2a), which is in accordance with our previous report, revealing the steady grafting of hydroxyl groups over the CNK and CNK−OH.[32] In particular, these peaks remain the same after the Fe^{3+} loading, which implied the stability of hydroxyl groups. As for ESR spectra (Figure 2b), there is no signal for the pristine CN whereas the CNK−OH presents typical signal correspond to DMPO−·OH adducts. For the sample CNK−OH, the ·OH can be generated via two routes, a direct holes oxidation of surface hydroxyl groups or a multistep photoreduction of O_2.[11] To rule out the possibility of latter, the suspension sample was purged with Ar for 10 min to eliminate the dissolved O_2. However, the 1:2:2:1 quartet signal that could be indexed as the DMPO−·OH adducts formed upon trapping of ·OH by the DMPO molecules is almost the same as the unpurged suspension with CNK−OH. Although the potential of valence-band edge of C_3N_4 is usually located at 1.2−1.6 eV[34,35] which thermodynamically disfavors for the oxidation level of OH^- (∼1.98 V vs NHE),[36] the conversion of grafted hydroxyl group into ·OH indeed occurs over CNK−OH, which can be ascribed to that the steady chemisorption of reactant over catalyst is beneficial for carrier transfer and thus decrease the thermodynamic requirement, just as the report of O_2 activation over O defect-rich WO_3 by Zhang et al.[37] The grafting position of hydroxyl group over C_3N_4 has been explored in detail in our previous study, which is also exhibited in Figure 3. Interestingly, the

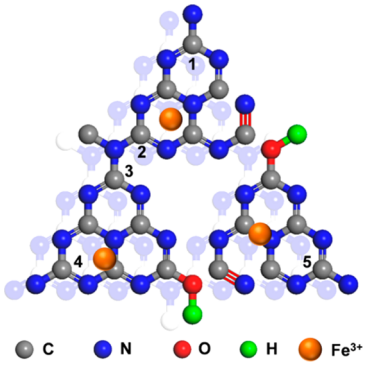

Figure 3. Chemical structure of CNK−OH&Fe. Note: the carbon atoms labeled by numbers are the adsorption sites of O_2 molecules.

single-line signal with a g value of 2.0025 decreased sharply when suspension sample was purged with sufficient Ar (Figure 2b), which reveals the adsorption site of O_2 molecule and will be discussed in detail later. Beyond that, the intuitive pH detection of CNK−OH further illustrates the alkalinity of this sample (Figure S3). The above-mentioned characterizations clearly evidence that the hydroxyl groups are indeed grafted over g-C_3N_4 samples.

For CNK−OH&Fe sample, X-ray photoelectron spectra (XPS) were recorded to determine the chemical state of the surface Fe species. In the Fe *2p* core level spectrum, the peak observed at 711.04 eV can be assigned to Fe^{3+} (Figure 4a).[38] In further ESR analysis, the figures of the two spectra are different, which can be attributed to different structural and chemical environment of Fe ions in CNK−OH&Fe and $FeCl_3$; however, the similar g values of both spectra reveal that CNK−OH&Fe presents strong Fe^{3+} signal as that in $FeCl_3$ (Figure 4b), which lends support to the XPS results illustrated above. Microstructures of the as-prepared samples were observed by scanning electron microscopy (SEM) and transmission electron

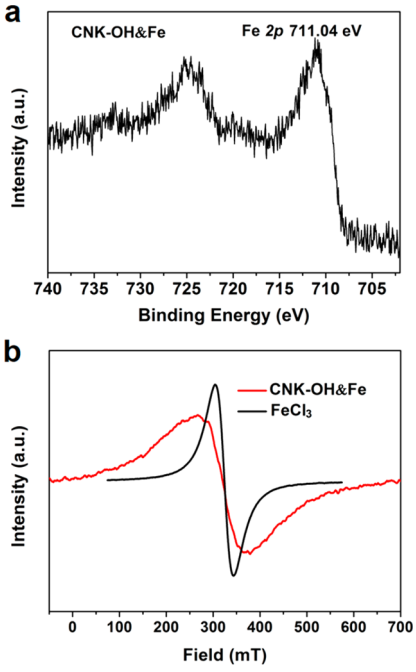

Figure 4. (a) The XPS spectrum of Fe *2p* for CNK−OH&Fe. (b) Comparison of ESR spectra of iron ions in CNK−OH&Fe and $FeCl_3$.

microscopy (TEM) (Figure S4). The K implantation as well as the hydroxyl group and Fe^{3+} modifications bring some effect of exfoliation and loosening on sample morphology, which thus enlarges the surface area (see details in Table S4). The TEM-EDS elemental mapping was used to further confirm the distribution of K, O and Fe (Figure S5). Overall characterizations as well as the analyses of XRD, FT-IR and XPS considered, K and O distributes homogeneously within the bulk and the shallow surface of sample particle, respectively; in view of the Fe^{3+} loading process, Fe^{3+} is mainly decorated in the shallow surface (as schematically shown in Figure 3).

CNK−OH&Fe Is about 270 Times More Active than Pristine C_3N_4. To assess the validity of the hydroxyl group and Fe^{3+} modification on improving photocatalytic efficiency, photocatalytic oxidation of isopropanol (IPA) was carried out over the as-synthesized photocatalysts. It is notable that the IPA photodegradation is an acknowledged model reaction for photooxidation of VOCs, since it includes both a single-photon route to generate the initial product of acetone and a multiphoton route to yield the complete degradation product of CO_2.[23,39] The optimal amount of added NaOH in feedstock was explored to be 0.125 g (Figure S6). Figure 5a presents the acetone and CO_2 production rates and the apparent quantum yield (AQY) at around 420 nm over each CNK−OH&Fe catalyst as a function of Fe^{3+} loading. The CNK−OH&Fe samples exhibit a hump-like photocatalytic activity depending on the loading amount of Fe^{3+} (with 1.4 wt% as an optimal amount). This phenomenon can be reasonably explained as that the increment of Fe^{3+} loading will promote the utilization of photoelectron (detailed mechanism study will be introduced in the next section) but also suppress the light absorption of semiconductor host, and thus, it should appear an optimal balance between these two contradictory factors at a certain loading amount of Fe^{3+} (1.4 wt%). Surprisingly, the IPA photooxidation rate over the best CNK−OH&Fe sample delivers an at least 2 orders of magnitude (∼270 folds) higher than that observed over pristine C_3N_4 and more than twice that

DOI: 10.1021/jacs.6b07272
J. Am. Chem. Soc. 2016, 138, 13289−13297

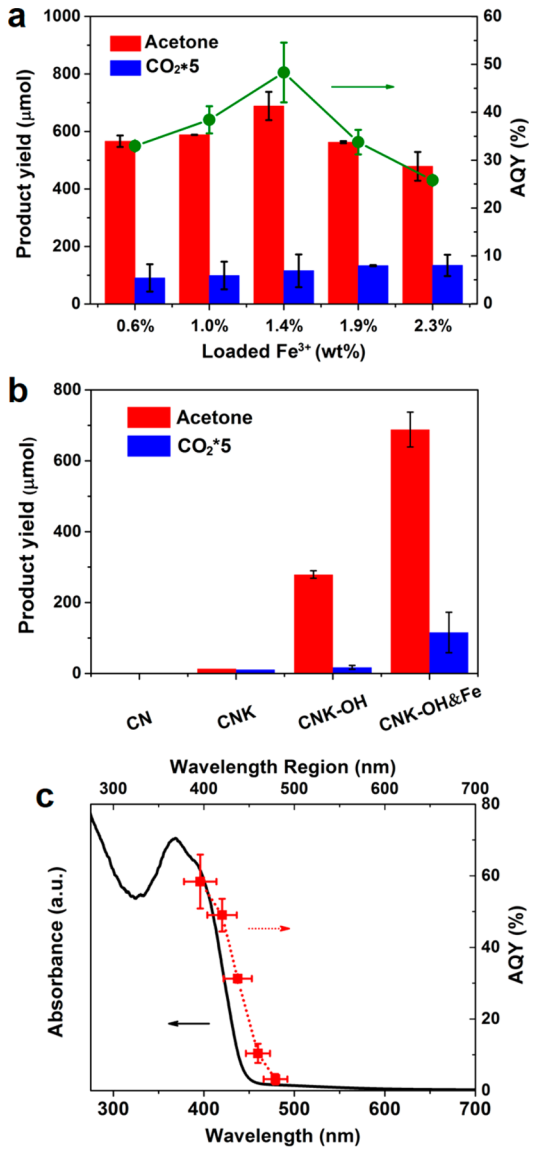

Figure 5. (a) Amounts of products yield and AQY over CNK−OH&Fe as a function of Fe^{3+} loading. (b) Photooxidation performance of C_3N_4-based photocatalysts. (c) Wavelength-dependent apparent quantum yield (AQY) of IPA photodegradation over CNK−OH&Fe at various light wavelength ranges consistent with the absorption spectrum.

of CNK−OH (Figure 5b). The specific results of typical IPA photooxidation are exhibited in Figure S7.

For the most active CNK−OH&Fe sample, the wavelength-dependent apparent quantum yield (AQY) is presented in Figure 5c (detailed data of measured photoactivity and light intensity are listed in Table S2), which is often used to distinguish whether the present chemical process is driven by photoinduced carrier or not.[39] The AQY decreases with increasing wavelength of the incident light, which tracks the optical absorption of the present sample. It suggests that the photophysical property of CNK−OH&Fe governs the chemical process of converting IPA into acetone and CO_2, and therefore, the present reaction primarily obeys semiconductor-based photocatalysis. The CNK−OH&Fe achieves a superior level of photooxidation with a high AQY of 49% at the wavelength of 420 ± 16 nm, which exceeds all the previously reported C_3N_4-based photocatalysts for gaseous pollutant degradation (see details in Supporting Information, Table S1).

For comparison, we measured the photoactivities of CNK−OH&Fe, commercial TiO_2 (P25) and self-prepared N doped TiO_2[40] (N-TiO_2, of which N doping concentration was optimized, see Figure S8) under solar simulator irradiation (AM 1.5). As shown in the Figure 6a,b, the acetone and CO_2 evolution rates over CNK−OH&Fe present obvious superiority among all three samples. The P25 and N-TiO_2 were also loaded with Fe^{3+} and then were measured the IPA photodegradation (Figure S1 and S9); however, only limited photoactivity enhancement is observed over the N-TiO_2 with Fe^{3+} loading (Figure S9). A long-term IPA photodegradation over the CNK−OH&Fe was also conducted under the visible-light irradiation (λ > 400 nm); the degradation and mineralization percentages of IPA was up to 99.9% in 20 min and 36 h, respectively (Figure S10). Cycle test of IPA photodegradation is used to evaluate the stability of CNK−OH&Fe, which will be discussed in detail in next section. To exclude the contribution come from Fe^{3+} or synergy between Fe^{3+} and OH, SiO_2−Fe and SiO_2−OH&Fe were synthesized. Compared with the CNK−OH&Fe, these two samples barely displayed photo-

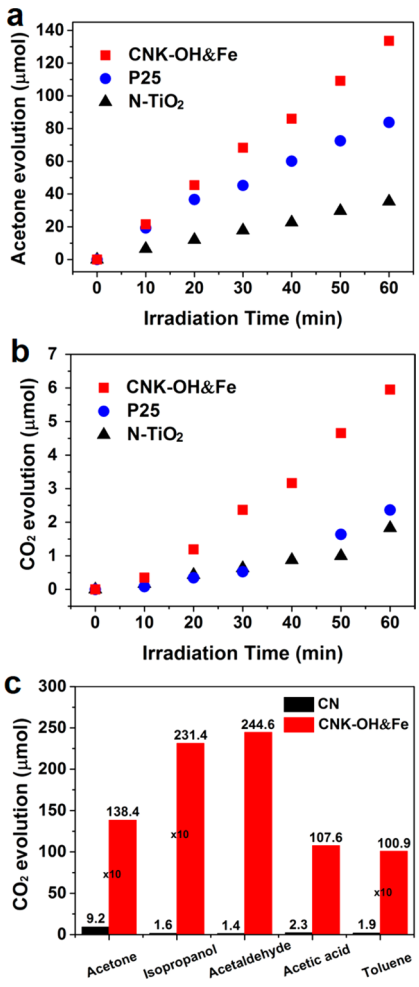

Figure 6. Comparison of acetone (a) and CO_2 (b) evolution over commercial TiO_2 (P25), N-TiO_2 and optimized CNK−OH&Fe sample under irradiation of simulated sunlight irradiation (AM 1.5, 100 mW cm^{-2}). (c) Comparison of CO_2 generation from various VOCs over CN and CNK−OH&Fe.

DOI: 10.1021/jacs.6b07272
J. Am. Chem. Soc. 2016, 138, 13289−13297

activity (Figure S11). Besides IPA, the CNK−OH&Fe photocatalyst also exhibits universal and efficient photoactivities to other VOCs, such as aldehyde, carboxylic acid, ketone, and aromatic hydrocarbon (Figure 6c). All above characterizations of catalytic efficiency demonstrate that the present photoreaction over CNK−OH&Fe is a high-efficient semiconductor-based photocatalytic process.

Light-Driven Fenton Reaction at Solid−Gas Interface. To gain insight into the enhancement of photocatalytic activity, we further explored the transfer and utilization of the photocarriers (photoexcited electrons and holes) in bulk and on surface of photocatalyst. Quick recombination of photocarriers is the main reason to limit the photocatalytic activity of C_3N_4.[41] However, the K implantation and the hydroxyl group modification can effectively improve the transfer efficiency and lifetime of photocarriers, which is evidenced via the synchronous illumination XPS (SIXPS),[42] photoelectrochemical and transient/steady-state fluorescence spectroscopy characterizations (see more details in Figure S12−S14, Table S3 and SI-2). These improvement approaches also influence the crystallinities, surface areas, light absorptions of photocatalysts and then enhance the photocatalytic activity, which but can be ruled out as the main factor (see details in Figure 1, Figure S15, Table S4, SI-3). As seen in Figure 5b, the surface modifications of hydroxyl group and Fe^{3+} play important roles in significantly promoting photoactivity, which can be ascribed to the construction of a new photochemical reaction route of light-driven Fenton reaction at solid−gas interface.

In traditional Fenton process, the H_2O_2 is one of the important reactants in the reactions as shown in eq 1, 2. In present system, the H_2O_2 is mainly produced via a route of photocatalytic O_2 reduction, which could be verified via measuring the amount of H_2O_2 yield over sample under the different atmospheres (Figure S16). To determine the generated H_2O_2 at photocatalyst-air solid−gas interface, we designed the experiment as following. The sample powder (10 mg) was irradiated under visible-light irradiation ($\lambda > 400$ nm) for 2 min with gaseous IPA addition and then was dispersed into distilled water; the filtrate of suspension was used to measure the amount of generated H_2O_2 via $KMnO_4$ titration method.[15,43] As presented in Figure 7a, the CN barely produce H_2O_2 (below detection limit, 0.2 μmol),[15] while the CNK−OH quickly generated ca. 3.4 μmol of H_2O_2; the evolved H_2O_2 is difficult to be observed over CNK−OH&Fe (below detection limit, 0.2 μmol), which can be reasonably explained that the generated H_2O_2 quickly reacts with Fe^{2+}, which derives from Fe^{3+} reduced by photoelectron to form ·OH (as eq 1). In the case of experiments in absence of gaseous IPA, the amounts of H_2O_2 yield over the three photocatalysts (which were measured with DPD method[44,45]) present the same variation tendency (Figure S17). To evidence the conversion of H_2O_2 into ·OH over CNK−OH&Fe, the ESR measurements under visible-light irradiation were performed. Besides the direct ·OH formation of surface hydroxyl oxidized by photoexcited hole as over CNK−OH sample, the CNK−OH&Fe opens the route of Fe^{2+}-induced H_2O_2 converting into ·OH. Therefore, as exhibited in Figure 7b, the amount of generated ·OH over CNK−OH&Fe is almost four times that over CNK−OH (the amount of free radical is approximatively proportional to the square of the height of signal). Furthermore, the amount of evolved H_2O_2 over CNK−OH&Fe was estimated to be 522 μmol/h (see more details in Supporting Information, Figure S18) and thus increased the corresponding amount of ·OH and

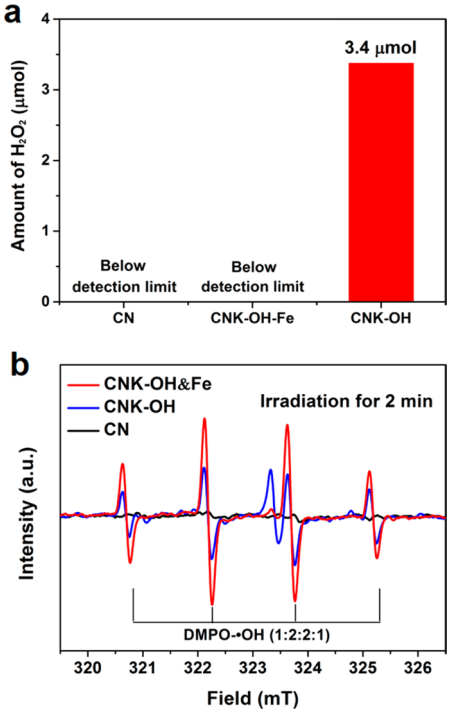

Figure 7. (a) H_2O_2 production of C_3N_4-based samples. Notes: samples were first irradiated with gaseous IPA, then they were dispersed into distilled water, finally the filtrates of suspensions were detected H_2O_2 by redox titration with $KMnO_4$ (detection limit: 0.2 μmol). (b) Comparison of ESR intensity of DMPO−·OH of a group of samples.

$\cdot O_2^-$ radicals, which is roughly consistent with the enhanced photoactivity (increased 409 μmol/h of acetone and 19.7 μmol/h of CO_2, which amounts to ∼527 μmol/h of utilized photon number) compared with the CNK−OH sample, implying the process of Fe^{2+}/Fe^{3+}-induced H_2O_2 converting into $\cdot OH/\cdot O_2^-$. Since the above-mentioned characterizations are aqueous-mediated measurements, it is necessary to rule out the possibility of Fenton reaction occurring in the aqueous phase. The control experiments were designed as following. The 2.5 mg of CNK−OH&Fe was added into a solution contained 0.8 μmol of H_2O_2 and then measured by DPD method, which is compared with the result that a solution contained 0.8 μmol of H_2O_2 was directly measured by DPD method (Figure S19). It is apparent that no any H_2O_2 in aqueous solution was consumed by Fe^{3+} of CNK−OH&Fe sample, indicating the present Fenton reaction indeed happens at solid−gas interface. For high-efficient Fenton process in the aqueous phase, the acid environment is indispensable,[26−28] which can explain that the above-mentioned reaction does not initiate; however, the solid−gas-interfacial Fenton reaction seems not to depend on the acid medium, and contrarily, the surface of CNK−OH&Fe sample presents alkaline property (Figure S3). Actually, the alkalinized surface (grafting of hydroxyl groups) is essential factor to construct an efficient solid−gas-interfacial Fenton process, since simple Fe^{3+} modification over semiconductor exhibits limited enhancement or even reduction effect on photoactivity (Figure S1). The detailed mechanism will be discussed in latter part.

The reactive oxygen-related species in the photooxidation process is one of the most concerning issues. Herein, we further studied the active species of CNK−OH and CNK−OH&Fe for

DOI: 10.1021/jacs.6b07272
J. Am. Chem. Soc. 2016, 138, 13289−13297

gaseous IPA photodegradation via a method of introducing scavengers. The *p*-benzoquinone (pBQ), coumarin (Cou) were adopted and served as the scavengers for $\cdot O_2^-$ and ·OH, respectively.[46,47] For the CNK−OH sample, only hole-induced ·OH participates the IPA photooxidation, since the Cou addition blocks this process while the pBQ introduction can consume photoelectrons and thus slightly promote the generation of ·OH as well as photoactivity (Figure 8a).

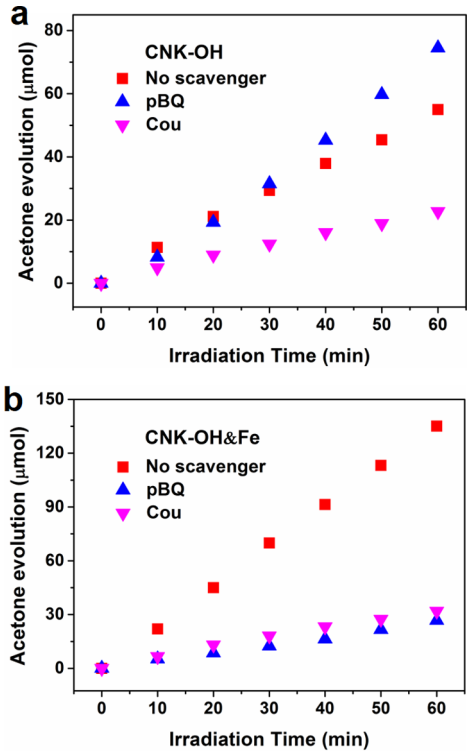

Figure 8. IPA photodegradation with different reactive-species scavengers. Before Fe^{3+} loading (a) and after Fe^{3+} loading (b).

Apparently, over the CNK−OH&Fe sample, both hole-induced ·OH and electron-induced ·OH/$\cdot O_2^-$ join the IPA photooxidation, because either the Cou addition or the pBQ introduction obviously suppresses the photoactivity (Figure 8b). Further careful comparison, when Cou was added, the photoactivity for converting IPA into acetone was reduced about 103 μmol for CNK−OH&Fe while only 33 μmol for CNK−OH (Figure 8a,b). It means that the amount of ·OH increased more than 3-fold with the assistance of Fe^{3+}, which is consistent with the results from the ESR method (Figure 7b). Interestingly and importantly, compared to CNK−OH, the photoactivity reverse (notable decrease) over the CNK−OH&Fe sample in the presence of the pBQ scavenger (Figure 8a,b) clearly indicates that the Fenton process coupled in photocatalytic reaction effectively converts photoelectrons into active radicals.

According to all above-mentioned results and discussions, the transfer routes of photocarriers in gaseous IPA degradation over CNK−OH&Fe as well as CNK−OH are summarized in Scheme 1, which helps to easily understand the efficient generation of active radicals via the solid−gas interfacial Fenton process. For CNK−OH, the active radicals are only generated from the single channel of photoholes while the photoelectrons are mainly consumed to form H_2O_2 which is inactive for IPA oxidation. However, in the case of CNK−OH&Fe, the channel of photoelectrons is also opened to produce reactive radicals including both ·OH and $\cdot O_2^-$ through Fenton process, which significantly increases the amount of active radicals (Figure 7b) and therefore greatly enhances photoactivity (Figure 5b). It is worth further clarifying two more keys about photocarrier transfer. First, as shown in Figure S20, the single-line signal (g = 2.0025) corresponds to the unpaired electron on carbon atom of the aromatic rings within π-bonded nanosized cluster;[48] probably, it is also the main form of trapped photoelectrons. Although the O_2 molecule exhibits effective adsorption on such carbon atoms (Figure 3) and efficient unfastening of these electrons to activate itself (Figure 2b, Figure S16 and Figure S20b), the Fe^{3+} loading presents further extract this type of electrons to form Fe^{2+}/Fe^{3+} pair and therefore contributes to more generation of reactive radicals (Figure 7b). Second, as aforementioned, the alkalinized surface (grafting of hydroxyl groups) plays a significant role in constructing efficient solid−gas-interfacial Fenton process. Actually, these surface hydroxyl species finally are converted into ·OH through the channel of photoholes and then oxidize the IPA to produce H^+; after that, the H^+ will participate to form H_2O_2. Hence, the promoted activity from the addition of Fe^{3+} is limited by the concentration of surface hydroxyl species and strongly depends on its related H_2O_2 generation amount (Figure 2a and Figure S21a), which further lends support to the proposed transfer routes of photocarriers and the Fenton process in the photocatalytic reaction (Scheme 1). Moreover, the consumption of surface hydroxyl species is also one of the most concerning issues. To reveal this underlying question, cycle test of IPA photodegradation and XPS measurement for CNK−OH&Fe before and after reaction were carried out. The cycle

Scheme 1. Proposed Mechanism of O-Related Radicals Generation in Photocatalytic Systems without (CNK−OH) and with Solid-Gas Interfacial Fenton Reaction Coupling (CNK−OH&Fe)

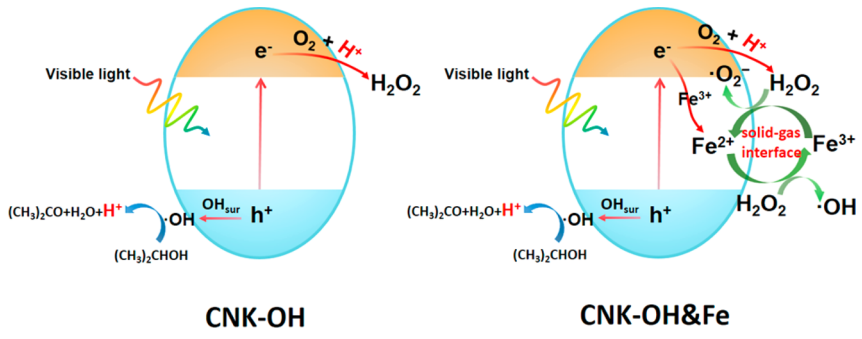

DOI: 10.1021/jacs.6b07272
J. Am. Chem. Soc. 2016, 138, 13289−13297

test indicates that the photoactivity of CNK−OH&Fe exhibits a continuous decline but the decay pace becomes slow (Supporting Information, Figure S22). The total amount of generated acetone in five cycles is 2.16 mmol which is much higher than the amount of grafted hydroxyl group over the initial photocatalyst (about 33.8 μmol in 50 mg of sample, which is calculated via XPS measurement in Table S5). Thereby, it can be inferred that the surface hydroxyl species could be self-regenerated during the photocatalytic process. However, it is also found that the amount of surface-anchored hydroxyl groups shows continuous decrease as 39% and 68% of reduction after one cycle and four cycles, respectively. Therefore, the photoactivity decay of CNK−OH&Fe can be partially attributed to the decrease of surface-grafted hydroxyl groups. The suitable activation process to recover the efficient photocatalytic activity is still under exploration.

CONCLUSIONS

In conclusion, our study demonstrates that a solid−gas-interfacial Fenton reaction can be constructed via modifying hydroxyl and Fe^{3+} species over g-C_3N_4-based photocatalyst. The photooxidations of volatile organic compounds over this photocatalyst are significantly boosted. Taking isopropanol photodegradation as an example, a more than 2 orders of magnitude greater than that proceed over pristine C_3N_4 is achieved, which corresponds to a high quantum yield of 49% at around 420 nm. The enhanced photoactivity can be attributed to the efficient conversion of photoexcited electron into reactive radicals (such as ·OH and $\cdot O_2^-$) through the solid−gas interfacial Fenton process. The hydroxyl and Fe^{3+} species in photoreaction play significant roles in in-situ H^+ production and Fe^{2+}/Fe^{3+} pair formation, respectively, and therefore determine the generation rate of H_2O_2 and active radicals, which are of crucial importance to construct this efficient Fenton reaction. We anticipate that the findings are not unique to C_3N_4, and any other semiconductors that could be surface-alkalinized (for example, WO_3,[49] $SrTiO_3$[50]) should deliver the same light-driven Fenton process, which opens a low-cost and facile way to efficiently eliminate gaseous organic contaminant using solar energy.

EXPERIMENTAL SECTION

Preparation of the Samples. The pristine g-C_3N_4 was fabricated using method as our previously report,[32] melamine was placed in crucible and heated up to 550 °C for 4 h at a rate of 2.3 °C min^{-1}. The sample obtained was named as CN. To synthesize the K implanted and hydroxyl grafted C_3N_4 (CNK−OH), typically, melamine (1.5 g; ≥ 99.0%), KCl (7.5 g, ≥ 99.5%) and NaOH (varied in the range of 0.05−0.20 g; ≥ 98.0%) were mixed fully by grinding. After calcination treatment, the powders were washed fully with distilled water until the supernatant was close to neutralization. Then, the resulting powders were dried at 80 °C overnight. Further Fe^{3+} modified sample (CNK−OH&Fe) was prepared by an impregnation method over the CNK−OH. Briefly, 60 mg of CNK−OH was first dispersed in 30 mL of distilled water. Dilute solution of $FeCl_3{\cdot}6H_2O$ (99.0%) was slowly added dropwise into the above solution. The weight of fraction of Fe^{3+} relative to g-C_3N_4 varied from 0.6 wt% to 2.3 wt%. The suspension was stirred for 24 h at room temperature and then dried at 80 °C. Note: CNK−OH&(Fe) in text refers to the sample synthesized with 0.125 g NaOH or 1.4 wt% Fe^{3+} as well, unless otherwise specified.

For comparison, N-TiO_2 powders were synthesized by annealing anatase TiO_2 (ST01) under NH_3 flow (50 mL/min) at 450, 500, and 550 °C for 3 h. The final product named as N-TiO_2/x was obtained, wherein x represents the annealing temperature. The photoactivities of those samples are compared in Figure S8.

The C_3N_4-based photocatalysts anodes were prepared via a spin-coating method. The samples were first dispersed into ethanol to form dispersion and then were spin-coated on FTO substrate layer by layer. Finally, the coated films were heated up to 350 °C with a temperature ramp of 5 °C min^{-1} and kept for 1 h under Ar atmosphere.

Characterization. XRD patterns of the as-prepared samples were collected with a powder X-ray diffractometer (Cu Kα radiation source, D8 Advanced, Bruker, Germany). UV−visible (UV−vis) diffuse reflectance spectra of the samples were recorded on a UV−visible spectrophotometer (UV-2700, Shimadzu, Japan) equipped with an integrating sphere, then converted into absorption spectra by Kubelka−Munk transformation. Specific surface areas were measured by nitrogen physisorption (Autosorb-iQ2, Quantachrome, America), and were calculated via the Brunauer−Emmett−Teller (BET) method. Infrared transmission spectra were used to detect hydroxyl group on the surface of samples; the spectra were collected using a Fourier Transform infrared (FTIR) spectrophotometer (Nicolet 6700, Thermo SCIENTIFIC, America). The Photoluminescence (PL) properties were investigated using a fluorescence spectrophotometer (Fluorolog-3, HORIBA Scientific, America). X-ray photoelectron spectroscopy (XPS) measurements were carried out on XPS instrument (Escalab 250, Thermo SCIENTIFIC, America). All binding energies were referenced to the C 1s peaks of the surface adventitious carbon at 284.8 eV. Synchronous illumination XPS (SIXPS) was conducted on XPS instrument (Escalab 250Xi, Thermo SCIENTIFIC, America) and a 300 W Xe arc lamp acted as illumination source. The changes of XPS spectra were obtained via controlling light on or off at given time intervals in the process of measurements. The electron spin resonance (ESR) measurements were performed on an ESR spectrometer (JES-FA 200, JEOL, Japan) with a modulation frequency of 100 kHz and a microwave power of 1.0 mW. A 500 W high-pressure mercury lamp equipped with a cutoff filter (420 nm < λ < 800 nm) was adopted as the illumination source for in situ ESR measurements. The photoelectrochemical properties of samples were examined with an electrochemical station (CHI 660e, CH instruments, China). The morphologies of samples were characterized with Field Emission Scanning Electron Microscope (S4800, HITACHI, Japan) and Transmission Electron Microscope (TEM) (Tecnai G2 F20, FEI, Holland).

Photocatalytic Activity Evaluation. A 300 W Xe arc lamp (21 A imported current; focus through a 45 × 45 mm shutter window) equipped with an L42 cutoff filter (λ > 400 nm) was employed as the light source. A 50 mg of as-prepared catalyst was spread evenly on a plate (area, 7.1 cm^2). Then the vessel was pretreated by artificial air [$V(O_2)$:$V(N_2)$ = 1:4] for 5 min to remove the gaseous impurities. The isopropanol (IPA) (ca. 1000 μmol) was injected into the vessel. Then the vessel was kept in the dark until ensuring an adsorption−desorption equilibrium of IPA on the sample before irradiation. The sacrificial agent experiments were conducted in the same procedure except the light intensity (10 A imported current) and the addition of sacrificial agent (see details sacrificial agent confirmation section in text). A gas chromatograph (GC-2014, Shimadzu Corp., Japan) equipped with methanizer and FID detector was used to detect the concentrations of IPA, acetone and CO_2. The apparent quantum efficiency (AQY) was measured under similar conditions except for the light intensity and the wavelength regions of the irradiation light. A set of glass filters consisting of band-pass and cutoff filters were adopted to control the wavelength regions of incident light. The irradiation lasted for 60 min for every wavelength region. The average intensity of irradiation was determined by using a spectroradiometer (AvaSolar-1, Avantes, America). The IPA photooxidation undergoes two kinds of typical reaction processes as below:

(1) One-photon reaction

$$CH_3CHOHCH_3 + e^- + O_2 + H^+ \rightarrow CH_3COCH_3 + \cdot OH + H_2O$$

$$\text{or } CH_3CHOHCH_3 + \cdot OH(h^+ + OH^-) \rightarrow CH_3COCH_3 + H_2O + H^+ + e^-$$

DOI: 10.1021/jacs.6b07272
J. Am. Chem. Soc. 2016, 138, 13289−13297

(2) Multiphoton reaction

$$CH_3CHOHCH_3 + 18{\cdot}OH(h^+ + OH^-) \rightarrow 3CO_2 + 13H_2O$$

Therefore, the AQY was calculated as the following equation,

$$AQY = [N(\text{acetone}) + N(CO_2) \times 6]/N(\text{photons}) \times 100\%$$

Note: N(acetone), $N(CO_2)$, and N(photons) refer to the molecular number of generated acetone, the molecular number of generated CO_2, and the number of incident photons in unit time, respectively. The amount of generated H_2O_2 in photoreaction was measured via $KMnO_4$ titration method or DPD method (see Supporting Information, SI-1).

■ ASSOCIATED CONTENT

Supporting Information

The Supporting Information is available free of charge on the ACS Publications website at DOI: 10.1021/jacs.6b07272.

Additional experimental method about measurement of H_2O_2, supplementary discussion about construction of quick transfer and conversion channel for photocarrier, supplementary discussion about noncritical factors in photocatalytic reaction, and additional experimental data and figures. (PDF)

■ AUTHOR INFORMATION

Corresponding Authors

*oysx@tju.edu.cn

*jinhua.ye@nims.go.jp

Notes

The authors declare no competing financial interest.

■ ACKNOWLEDGMENTS

This work received financial support from the National Basic Research Program of China (973 Program, No. 2014CB239301), National Natural Science Foundation of China (21573158, 51502200, 51502198), Natural Science Foundation of Tianjin (15JCYBJC17400 and 15JCQNJC03500). S. O. thanks the financial support from the "Peiyang Young Researcher" Program of Tianjin University (No.2015XRX-0019).

■ REFERENCES

(1) Chen, X.; Shen, S.; Guo, L.; Mao, S. S. *Chem. Rev.* **2015**, *110*, 6503−6570.

(2) Tong, H.; Ouyang, S.; Bi, Y.; Umezawa, N.; Oshikiri, M.; Ye, J. *Adv. Mater.* **2012**, *24*, 229−251.

(3) Habisreutinger, S. N.; Schmidt-Mende, L.; Stolarczyk, J. K. *Angew. Chem., Int. Ed.* **2013**, *52*, 7372−7408.

(4) Hoffmann, M. R.; Martin, S. T.; Choi, W.; Bahnemann, D. W. *Chem. Rev.* **1995**, *95*, 69−96.

(5) Wang, X.; Maeda, K.; Thomas, A.; Takanabe, K.; Xin, G.; Carlsson, J. M.; Domen, K.; Antonietti, M. *Nat. Mater.* **2009**, *8*, 76−80.

(6) Wang, X.; Maeda, K.; Chen, X.; Takanabe, K.; Domen, K.; Hou, Y.; Fu, X.; Antonietti, M. *J. Am. Chem. Soc.* **2009**, *131*, 1680−1681.

(7) Liu, G.; Niu, P.; Sun, C.; Smith, S. C.; Chen, Z.; Lu, G.; Cheng, H. *J. Am. Chem. Soc.* **2010**, *132*, 11642−11648.

(8) Liu, G.; Wang, T.; Zhang, H.; Meng, X.; Hao, D.; Chang, K.; Li, P.; Kako, T.; Ye, J. *Angew. Chem., Int. Ed.* **2015**, *54*, 13561−13565.

(9) Zhang, G.; Zang, S.; Wang, X. *ACS Catal.* **2015**, *5*, 941−947.

(10) Yan, S.; Li, Z.; Zou, Z. *Langmuir* **2009**, *25*, 10397−10401.

(11) Yan, S.; Li, Z.; Zou, Z. *Langmuir* **2010**, *26*, 3894−3901.

(12) Zheng, Y.; Lin, L.; Ye, X.; Guo, F.; Wang, X. *Angew. Chem., Int. Ed.* **2014**, *53*, 11926−11930.

(13) Yu, J.; Wang, K.; Xiao, W.; Cheng, B. *Phys. Chem. Chem. Phys.* **2014**, *16*, 11492−11501.

(14) Chen, X.; Zhang, J.; Fu, X.; Antonietti, M.; Wang, X. *J. Am. Chem. Soc.* **2009**, *131*, 11658−11659.

(15) Shiraishi, Y.; Kanazawa, S.; Kofuji, Y.; Sakamoto, H.; Ichikawa, S.; Tanaka, S.; Hirai, T. *Angew. Chem., Int. Ed.* **2014**, *53*, 13454−13459.

(16) Sun, J.; Zhang, J.; Zhang, M.; Antonietti, M.; Fu, X.; Wang, X. *Nat. Commun.* **2012**, *3*, 1139.

(17) Zhang, J.; Zhang, M.; Yang, C.; Wang, X. *Adv. Mater.* **2014**, *26*, 4121−4126.

(18) Jin, Z.; Murakami, N.; Tsubota, T.; Ohno, T. *Appl. Catal., B* **2014**, *150*−*151*, 479−485.

(19) Jiang, H.; Liu, G.; Wang, T.; Li, P.; Lin, J.; Ye, J. *RSC Adv.* **2015**, *5*, 92963−92969.

(20) Sano, T.; Tsutsui, S.; Koike, K.; Hirakawa, T.; Teramoto, Y.; Negishi, N.; Takeuchi, K. *J. Mater. Chem. A* **2013**, *1*, 6489−6496.

(21) Ma, J. Z.; Wang, C. X.; He, H. *Appl. Catal., B* **2016**, *184*, 28−34.

(22) Zhao, J.; Wu, T.; Wu, K.; Oikawa, K.; Hidaka, H.; Serpone, N. *Environ. Sci. Technol.* **1998**, *32*, 2394−2400.

(23) Arsac, F.; Bianchi, D.; Chovelon, J.; Ferronato, C.; Herrmann, J. *J. Phys. Chem. A* **2006**, *110*, 4202−4212.

(24) Brillas, E.; Sirés, I.; Oturan, M. A. *Chem. Rev.* **2009**, *109*, 6570−6631.

(25) Pignatello, J. J.; Oliveros, E.; MacKay, A. *Crit. Rev. Environ. Sci. Technol.* **2006**, *36*, 1−84.

(26) Brillas, E.; Mur, E.; Sauleda, R.; Sànchez, L.; Peral, J.; Domènech, X.; Casado, J. *Appl. Catal., B* **1998**, *16*, 31−42.

(27) Wang, S. *Dyes Pigm.* **2008**, *76*, 714−720.

(28) Luo, W.; Zhu, L.; Wang, N.; Tang, H.; Cao, M.; She, Y. *Environ. Sci. Technol.* **2010**, *44*, 1786−1791.

(29) Morikawa, T.; Ohwaki, T.; Suzuki, K.-I.; Moribe, S.; Tero-Kubota, S. *Appl. Catal., B* **2008**, *83*, 56−62.

(30) Ohwaki, T.; Shu, S.; Aoki, K.; Morikawa, T. *Jpn. J. Appl. Phys.* **2016**, *55*, 01AA05.

(31) Thomas, A.; Fischer, A.; Goettmann, F.; Antonietti, M.; Müller, J.-O.; Schlögl, R.; Carlsson, J. M. *J. Mater. Chem.* **2008**, *18*, 4893−4908.

(32) Li, Y.; Xu, H.; Ouyang, S.; Lu, D.; Wang, X.; Wang, D.; Ye, J. *J. Mater. Chem. A* **2016**, *4*, 2943−2950.

(33) Sharma, J.; Gora, T.; lRimstidt, J.; Staley, R. *Chem. Phys. Lett.* **1972**, *15*, 232−235.

(34) Cui, Y.; Ding, Z.; Liu, P.; Antonietti, M.; Fu, X.; Wang, X. *Phys. Chem. Chem. Phys.* **2012**, *14*, 1455−1462.

(35) Yu, W.; Xu, D.; Peng, T. *J. Mater. Chem. A* **2015**, *3*, 19936−19947.

(36) Dang, X.; Zhang, X.; Zhang, W.; Dong, X.; Wang, G.; Ma, C.; Zhang, X.; Ma, H.; Xue, M. *RSC Adv.* **2015**, *5*, 15052−15058.

(37) Zhang, N.; Li, X.; Ye, H.; Chen, S.; Ju, H.; Liu, D.; Lin, Y.; Ye, W.; Wang, C.; Xu, Q.; Zhu, J.; Song, L.; Jiang, J.; Xiong, Y. *J. Am. Chem. Soc.* **2016**, *138*, 8928−8935.

(38) Choudhury, T.; Saied, S.; Sullivan, J.; Abbot, A. *J. Phys. D: Appl. Phys.* **1989**, *22*, 1185−1195.

(39) Ouyang, S.; Ye, J. *J. Am. Chem. Soc.* **2011**, *133*, 7757−7763.

(40) Irie, H.; Watanabe, Y.; Hashimoto, K. *J. Phys. Chem. B* **2003**, *107*, 5483−5486.

(41) Wang, Y.; Wang, X.; Antonietti, M. *Angew. Chem., Int. Ed.* **2012**, *51*, 68−89.

(42) Liu, X.; Dong, G.; Li, S.; Lu, G.; Bi, Y. *J. Am. Chem. Soc.* **2016**, *138*, 2917−2920.

(43) Zhuang, H.; Yang, L.; Xu, J.; Zhang, Z.; Lin, H.; Long, J.; Wang, X. *Sci. Rep.* **2015**, *5*, 16947.

(44) Bader, H.; Sturzenegger, V.; Hoigne, J. *Water Res.* **1988**, *22*, 1109−1115.

(45) Liu, G.; Wang, T.; Ouyang, S.; Liu, L.; Jiang, H.; Yu, Q.; Kako, T.; Ye, J. *J. Mater. Chem. A* **2015**, *3*, 8123−8132.

(46) Lin, Y.; Li, D.; Hu, J.; Xiao, G.; Wang, J.; Li, W.; Fu, X. *J. Phys. Chem. C* **2012**, *116*, 5764−5772.

(47) Wang, J.; Wang, K.; Wang, F.-B.; Xia, X.-H. *Nat. Commun.* **2014**, *5*, 5285.

(48) Zhang, J.; Zhang, G.; Chen, X.; Lin, S.; Mohlmann, L.; Dolega, G.; Lipner, G.; Antonietti, M.; Blechert, S.; Wang, X. *Angew. Chem., Int. Ed.* **2012**, *51*, 3183−3187.
(49) Kako, T.; Meng, X.; Ye, J. *Appl. Catal., A* **2014**, *488*, 183−188.
(50) Ouyang, S.; Tong, H.; Umezawa, N.; Cao, J.; Li, P.; Bi, Y.; Zhang, Y.; Ye, J. *J. Am. Chem. Soc.* **2012**, *134*, 1974−1977.

DOI: 10.1021/jacs.6b07272
J. Am. Chem. Soc. 2016, 138, 13289−13297